Optical Gating Electron Transport through Nonphotoresponisive Molecular Junctions

Zhikai Zhao
Key Laboratory of Optical Information Science and Technology, Institute of Modern Optics, Nankai University

Chengyang Guo
Key Laboratory of Optical Information Science and Technology, Institute of Modern Optics, Nankai University

Feng Sun
Shandong Normal University

Tingyin Ning
Shandong Normal University

Zongliang Li
College of Physics and Electronics

Bingqian Xu
University of Georgia

Xueyan Zhao
Nankai University

Lifa Ni
Key Laboratory of Optical Information Science and Technology, Institute of Modern Optics, Nankai University

Qingling Wang
Nankai University

Keehoon Kang
Seoul National University

Takhee Lee
Seoul National University https://orcid.org/0000-0001-5988-5219

Dong Xiang (xiangdongde@126.com)
Nankai University https://orcid.org/0000-0002-5632-6355

Article

Keywords: Single-molecule Junctions, Molecular Hybrid Devices, Nanogap Plasmons

Posted Date: September 18th, 2020

DOI: https://doi.org/10.21203/rs.3.rs-75718/v1

Optical Gating Electron Transport through Nonphotoresponisive Molecular Junctions

Zhikai Zhao[1,2], Chenyang Guo[1,2], Feng Sun[3], Tingyin Ning[3], Zongliang Li[3], Bingqian Xu[4], Xueyan Zhao[1], Lifa Ni[1], Qingling Wang[1], Keehoon Kang[1], Takhee Lee[2] & Dong Xiang[1]**

[1]Tianjin Key Laboratory of Micro-scale Optical Information Science and Technology, Institute of Modern Optics, College of Electronic Information and Optical Engineering, Nankai University, Tianjin 300350, China

[2]Department of Physics and Astronomy, Seoul National University, Seoul 08826, Korea

[3]School of Physics and Electronics, Shandong Normal University, Jinan 250014, China

[4]College of Engineering, University of Georgia, Georgia 30602, USA

Abstract: The manipulation of electron transport through single-molecule junctions *via* light illumination is a critical step towards molecular hybrid devices. However, most kinds of molecules are nonphotoresponsive without photo absorption upon a specific light illumination. Here, a strategy for high efficiently gating electron transport through a nonphotoresponsive molecular junction with a general light source is provided by introducing nanogap plasmons and molecular design. It is found the conductance of the triphenylamine-based molecules, a nonphotoresponsive molecule with buried anchoring groups, can be enhanced by two orders of magnitude under a general light illumination, which should be the greatest enhancement in the family of nonphotoresponsive molecules. It is further revealed that the giant conductance modulation originates from the coupling of the buried anchoring groups and plasmon-excited hot electrons. This work would contribute to the understanding of the interaction mechanisms between light and bridged molecules, assisting the development of the molecule-based hybrid optoelectronic devices.

The ability to control the electrical current through a molecule is a critical step to realize functional molecular devices[1-3]. A typical method to control the electronic transport through single molecules is to employ the strategy of a field-effect transistor, in which the molecular orbitals are energetically shifted by the gate voltage and thus the charge transport through the molecule is modulated[4]. Using light as an external stimulation to modulate electron transport through single molecules, like a solid field-effect transistor, have attracted growing intensive interests due to its potential applications in the fabrication of miniaturized hybrid optoelectronic devices. Furthermore, it provides a platform to investigate the interaction between light and matter at the molecular level[5,6]. However, the mismatch between the scale of optical waves and that of individual molecules presents an obstacle for achieving a high-efficiency modulation/strong interaction. Luckily, surface plasmon polaritons (SPPs), which merge electronics and photonics and can be confined to far subwavelength dimensions with high energy intensity, may offer a solution to this size-compatibility problem[7,8].

Regarding how the electron transport through single-molecule junctions is modulated by light, several mechanisms have been proposed, including photo-induced intramolecular structural change[9-14], photo-induced proton transfer (PIPT)[15], photo-assisted tunneling (PAT)[16-18], resonant optical transitions[19,20], and exciton binding[21]. A well-known mechanism is the conversion from photon energy to mechanical energy based on photochromic molecules, such as azobenzene[22,23], diarylethene[9,24], and spiropyran[12], which can be interconverted between bistable or multiple conformational states under illumination. The structural transformation induced by optical absorption

may result in a giant conductance change, making it feasible to fabricate molecular switches. PIPT can achieve photo responsiveness based on some special molecules and a photoacid solvent in which the molecule isomerizes and releases a proton upon illumination[15,25]. In this way, the conductance of the molecular junctions can be modulated by one order of magnitude[15]. The PAT mechanism (or Tien-Gordon theory) explains how a periodic voltage $V_{ac}(t)$ from the electric field of the light wave drives a periodic shift of the energies in the electron transmission function, *i.e.*, the photon energy is transferred to individual electrons[26,27]. It has been reported that the conductance of single-molecule junctions can be enhanced up to a factor of two by PAT[5]. Other mechanisms include, for example, the opening of additional conduction channels resulting from an inherent asymmetry in the molecular junction under a resonant optical illumination[20], and molecular orbitals reconstruction based on the formation of bound excitons under the resonance carriers' excitation[21,28]. These previously reports promote the understanding of the interaction of light and single molecules, and step forward to realize functional devices. One of the remaining challenges for optical controlling electron transport through single molecules is that most molecules are nonphotoresponisve, *i.e.*, they neither absorb the photon energy nor undergo a structural transformation upon specific light illumination. Therefore, it is greatly difficult to control electron transport through these kinds of molecules with a general light source. SPPs, which can be easily excited by scattered light in the nanogap without specific requirement for the incident light[29,30], combined with an appropriate anchoring group design may solve this knotty problem.

To date, anchoring groups such as thiol (-SH), amine (-NH_2), pyridine, and carboxylic acid (-COOH) have been extensively used because of their stable electrical coupling when in contact with metal leads. Normally, the stronger the bonding group, the larger the molecular conductance if the bonding group can achieve direct contact with the electrodes. However, there is also a large variety of molecules that possess strong anchoring groups buried in the molecule backbone (*i.e.*, the direct coupling between the anchoring group and electrodes is spatially blocked by, *e.g.*, the molecular branches), which will result in poor conductance of the junctions. We anticipate that the poor conductance of such molecular junctions might be dramatically improved under illumination if a strong coupling between the buried anchoring groups and electrodes can be established *via* tunneling plasmonics[31].

To prove this anticipation, we experimentally measured the conductance of triphenylamine-based molecular junctions, in which the direct coupling of the anchoring group and electrodes is unavailable under dark conditions. As expection, a poor conductance of the molecular junction is determined by analyzing the conductance histograms. Interestingly, upon light illumination, two additional dramatically enhanced conductance peaks appear in the conductance histogram for this nonphotoresponsive molecular junction. The three conductance peaks, in total, follow a log-linear relationship. We attribute these features to the interaction between surface plasmons and the molecules. Assisted by density functional theory (DFT) calculations, we demonstrate that the coupling of plasmon-excited hot electron and the buried anchoring groups is the reason for the dramatic conductance modulation.

Results and discussion

Experimentally, we employed a custom-designed MCBJ setup integrated with a laser source for addressing the charge transport properties of molecules. In brief, a notched pure gold wire (100 μm in diameter, approximately 10 mm in length) was fixed on top of a polyimide coated substrate and the substrate was subsquently mounted in a three-point bending configuration. The gold wire was elongated and then broken by mechanical bending of the substrate, and cleanly fractured surfaces of the gold wire were exposed. The bending could also be relaxed to form atomic-scale contacts again by the control of a piezo-element, see supplementary Fig. S1. A *p*-polarized He-Ne laser (λ= 632.8 nm), in which the electric field of the incident light is parallel to the electrode axis, was used as a light source to excite strong SPPs in the nanogap as described in our previous report[32].

By taking advantage of the knowledge of plasmon-induced transport properties of metal point contacts[27,32,33], we first investigated the electrical characteristics of bare gold electrodes with and without illumination in a shielding box. Figure 1a shows the statistical histograms with both linear coordinates and logarithmic coordinates in dark conditions. Figure 1b shows the corresponding results upon illumination. It can be found that the bare gold conductance displayed integer-multiple G_0 peaks in the histograms regardless of the illumination condition. The individual conductance traces show the same feature as well, see supplementary Fig. S2. Meanwhile, no extra peak below $1G_0$ was observed in the histograms irrespective of whether the bare metal junctions were illuminated or not (see logarithmic coordinates).

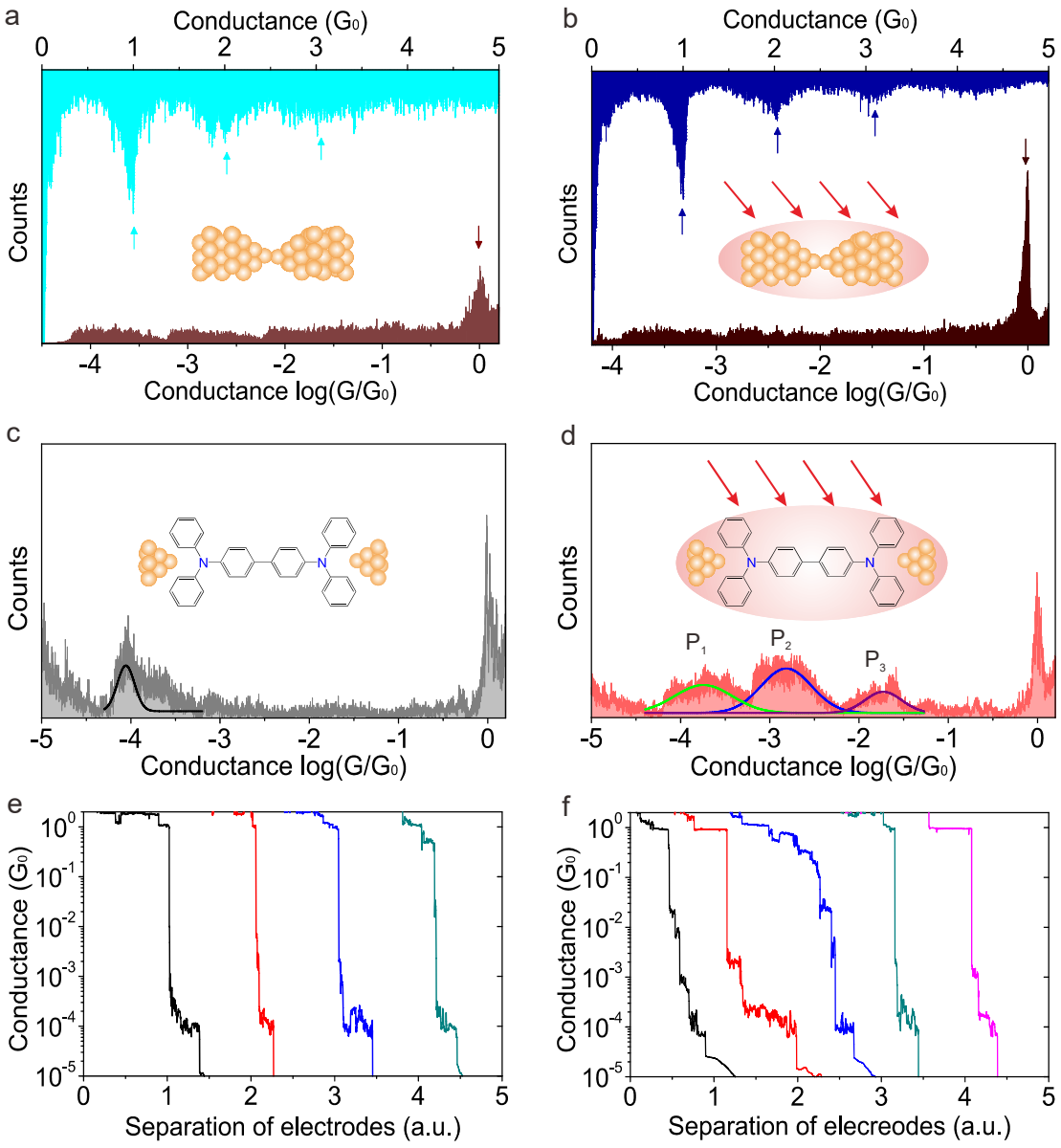

Fig. 1 | Conductance traces and histograms of the junctions with and without light illumination. **(a-b)** Linear and logarithm conductance histograms of bare gold wire (**a**) in dark and (**b**) upon illumination. **c** Conductance histogram of TPB molecules sandwiched between two electrodes in the absence of illumination with a Gaussian-fitted peak at approximately 8.8×10^{-5} G_0. Inset: Schematic of the molecular structure sandwiched between two separated electrodes. **d** Conductance histogram of TPB molecules in the presence of illumination, with three Gaussian-fitted peaks (P_1, P_2, and

P_3) at approximately 1.8×10^{-4} G_0, 1.5×10^{-3} G_0, and 1.9×10^{-2} G_0, respectively. (**e-f**) Logarithm conductance traces during the separation of the electrodes (**e**) without laser illumination and (**f**) in the presence of illumination.

Our previous work showed that the atomic-scale geometries of electrodes can tune the hybridization type of amine bond groups in 4,4′-diaminobiphenyl (DBP) molecular junctions[34]. In this work, the H atoms in the anchoring groups ($-NH_2$) at the ends of DBP were replaced by benzenes to generate the N,N,N',N′-tetraphenylbenzidine (TPB) molecular junctions, as shown in Fig. 1c. In this way, the direct coupling between the anchoring N atoms and electrodes is spatially hindered by the benzenes. A previous study showed that a strong UV-visible absorption only appeared approximately 299-351 nm for a triphenylamine-based molecule[35]. Our target molecule TPB, as one of the triphenylamine-based derivatives, shows a similar absorption peak wavelength smaller than 446 nm by both density functional theory (DFT) calculation and optical spectroscopy measurement, see supplementary Fig. S3. Our experiments were performed under light illumination with a 623.8 nm laser far from the absorption peaks, which means that the TPB molecules are unlikely to undergo an optical transition to an excited state by the optical absorption.

The TPB molecules were dissolved in an organic solvent (≈1 mM in tetrahydrofuran) and were self-assembled on gold contacts for 30 minutes after breaking the metal wire. The conductance traces were recorded in ambient conditions after drying the samples with nitrogen. The recorded conductance traces show a stepwise feature during the separation process, as expected. The plateaus located far

below G_0 indicate that the electrodes were bridged with the target molecules, and the lowest plateaus arose from the charge transport across a single TPB molecule bridged junction. Several representative traces recorded in dark are shown in Fig. 1e. The conductance histogram was created by five hundred conductance traces without data selecting. A peak located at approximately 8.8×10^{-5} G_0 can be observed in the conductance histogram, as shown in Fig. 1c.

We further recorded the conductance of the target molecule in the presence of illumination by focusing a 632.8 nm He-Ne laser at the junction region. From the analysis of the histogram presented in Fig. 1d, we obtained a completely different conductance profile with three peaks (P_1, P_2, and P_3) approximately 1.8×10^{-4} G_0, 1.5×10^{-3} G_0, and 1.9×10^{-2} G_0. Comparing these peaks with the one presented in Fig. 1c, two essential features can be observed. First, the peak (P_1) in Fig. 1d shifted to a little bit higher conductance value when the junction was illuminated. We attribute this observation to 1) plasmon-induced hot carriers directly transfer across the nanogap between electrodes[31,33,36,37], and 2) photo-assisted tunneling[5]. Both of them contribute a small proportion of the total current. Second, two additional peaks (P_2 and P_3) with much higher conductance values (up to 100 times larger) than P1 appeared upon illumination. These two additional peaks should not be caused by the hot carriers transferring across the nanogap, photo-assisted tunneling, or bound excitons as previously reported, since the conductance enhanced by them is rather limited, normally no more than a factor of two[5,21].

Considering the specific structure of the molecule, our observations may originate

from two paricular mechanisms: 1) The molecular conformation changes upon laser illumination, which may cause dramatic conductance changes. It has been reported that the conductance of a biphenyl molecular junction has a strong correlation with the internal twist angle between adjacent benzene rings in the molecular backbone[34]. If the two adjacent benzene rings rotate relative to each other, the degree of the π-conjugation between them will change, thereafter leading to a conductance change; 2) The coupling of the molecule-electrode at the two terminals is modulated upon illumination, which produces two extra peaks in the conductance histogram.

To determine which mechanism is responsible for the significant conductance modification, a further experiment was performed with N,N,N',N'-tetraphenylbenzene-1,4-diamine (TPD), whose molecular backbone includes only one benzene, as illustrated in the inset of Fig. 2. With this kind of molecule, the effect arising from the relative rotation of the two benzene rings along the molecule backbone can be excluded. Figure 2a and Fig. 2b show the conductance histogram of the molecular junctions in dark conditions and upon illumination, respectively. Figure 2a shows a peak located at approximately 2.8×10^{-4} G_0. In contrast, Fig. 2b presents three peaks (P_1', P_2' and P_3') located at approximately 3.0×10^{-4} G_0, 7.2×10^{-3} G_0, and 9.8×10^{-2} G_0, respectively. Figure 2c and Fig. 2d show several typical conductance traces during separation in dark conditions and under illumination. It can be found that the conductance traces presented in Fig. 2d show more steps compared to Fig. 2c, which is coherent with the histogram as presented in Fig. 2a and Fig. 2b.

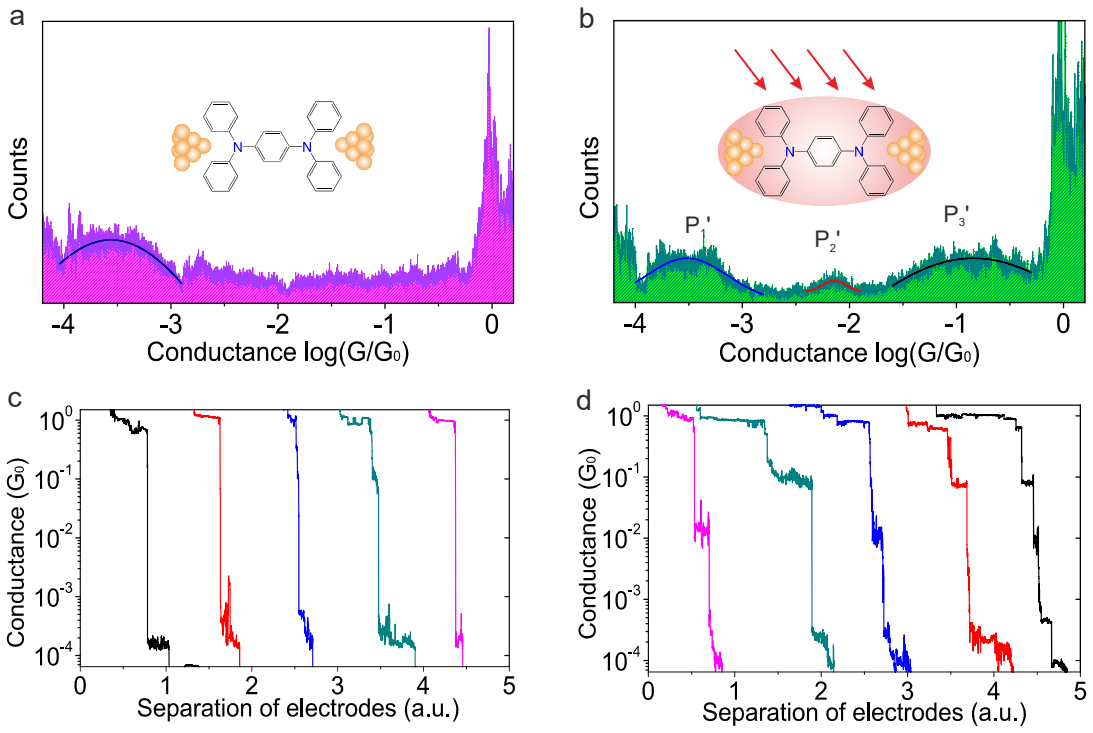

Fig. 2 | Conductance traces and histograms of the TPD junctions with and without light illumination. a Conductance histogram of TPD molecules in dark condition, with a Gaussian-fitted peak at approximately 2.8×10^{-4} G_0. The inset illuminates the molecular structure sandwiched between two separated electrodes. **b** Conductance histogram of TPD molecules upon illumination with three Gaussian-fitted peaks (P_1', P_2', and P_3') at approximately 3.0×10^{-4} G_0, 7.2×10^{-3} G_0, and 9.8×10^{-2} G_0, respectively. (**c-d**) Logarithm conductance traces during the separation of electrodes (**c**) without light illumination and (**d**) upon illumination.

Comparing these conductance histograms of TPD molecular junctions (Fig. 2a and 2b) with that of TPB molecular junctions (Fig. 1c and 1d), we found a common feature that there is only one obvious peak in the dark, while two additional peaks appear under illumination for both TPD and TPB junctions. We now turn to establish the relationship

between these peaks′ values. Interestingly, we found that the conductance values for both types of molecules followed $P_2 \approx \sqrt{P_1 \times P_3}$ upon illumination, where P_1, P_2, and P_3 are the minimal, middle, and maximal conductance values, respectively. The charge transport across a two-terminal molecular junction follows the Breit–Wigner formula[38].

$$T(E,V) = 4\Gamma_1\Gamma_2/\{[E - E_0(V)]^2 + [\Gamma_1 + \Gamma_2]^2\} \quad (1)$$

where $T(E,V)$ is the transmission coefficient of the electrons at an energy E under a bias V, and Γ_1 and Γ_2 describe the coupling of the molecular orbital to the left electrode and right electrode, respectively. E_0 is the eigenenergy of the molecular orbital which may be shifted slightly due to the coupling of the orbital to the electrodes[39]. In our cases, TPB and TPD molecules have a common anchoring group (triphenylamine), from which the molecule-electrode coupling strength is weak such that the last term of the denominator in the Breit-Wigner formula can be omitted. Thus, formula (1) can be simplified as:

$$T(E,V) \approx 4\Gamma_1\Gamma_2/[E - E_0(V)]^2 \quad (2)$$

The transmission of a symmetric molecule can have three possible states ($4\tau_1^2/[E - E_0(V)]^2$, $4\tau_1\tau_2/[E - E_0(V)]^2$, $4\tau_2^2/[E - E_0(V)]^2$) in cases of the molecule-electrode coupling strength being different at two ends (τ_1, τ_2 where $\tau_1 \neq \tau_2$) upon illumination. It can be found that these three transmission values follow the equation $T_2 \approx \sqrt{T_1 \times T_3}$, agreeing with experimental observations.

Subsequently, we try to address the coupling change between the target molecules and electrodes induced by the laser illumination. It has been reported that plasmon-excited nanoparticles or nanogaps can be an efficient source of hot electrons[40,41]. For

simplicity, we used nanoparticles instead of nanoelectrodes to schematically show the distribution of hot electrons. Figure 3a and 3b depict how plasmon excitation can create hot electrons on gold nanoparticle (Au NP) surfaces. Following the optical excitation, each plasmon quantum can decay into either a radiative photon (scattering) or a nonradiative electron-hole pair. For small nanostructures, a dominant decay channel is the electron-hole pair formation[42,43]. It has also been reported that as the nanogap between the electrodes decreases below a critical size, *e.g.*, less than 0.5 nm, the plasmon interactions enter a quantum conductive regime where the decay of the plasmons creates a distribution of hot electrons, which causes the transfer of electrons between the nanoelectrodes[31,44,45]. Weng *et al*. directly visualized hot-electron distributions in the junction regions *via* shot noise by using a scanning near-field optical microscope[46], which demonstrated that the hot electrons can be spatially diffused by fluctuating EM evanescent fields, see supplementary Fig. S4 for more details. All these reports indicate that the nanogap can host a large number of hot electrons, and hot electrons can extend further away from the nanoelectrodes, which may dramatically change the coupling state between electrodes and sandwiched molecules.

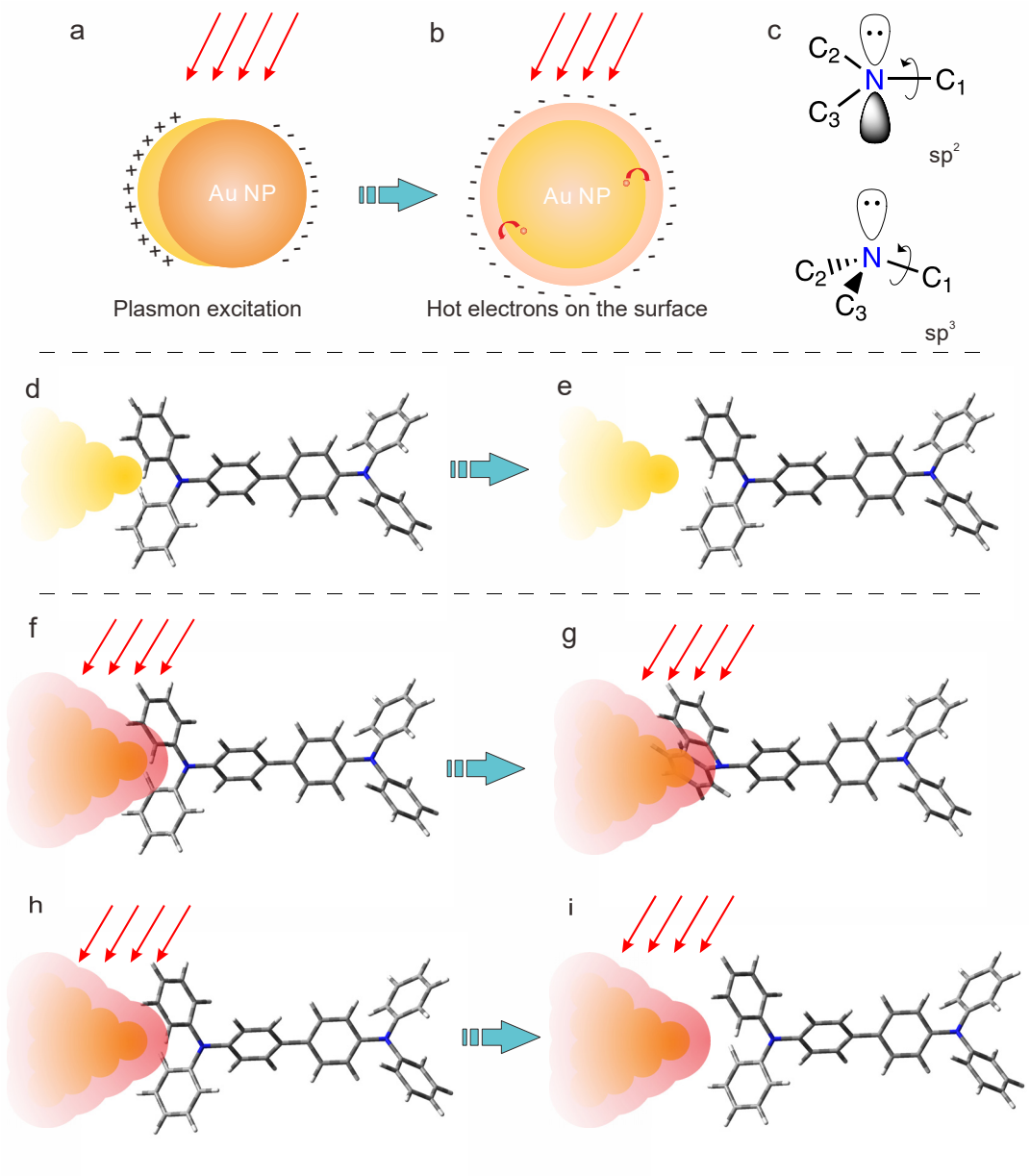

Fig. 3 | Schematics of the generation of hot electrons on gold nanoparticle surface and the change of orbital hybridization of N atom upon illumination. a Plasmon-excited gold nanoparticles as an efficient source of hot electrons. **b** The expanded distribution of hot electrons on the surface of the nanoparticles. **c** The dihedral angle of N atom in sp^2(180°) and sp^3(120°) hybridization state. **d** The initial junction structure without laser illumination. Only one electrode is shown in the molecule junction. **e** The breaking of the molecular junction during the stretching process in the dark. **f** The

distribution of hot electrons expanded beyond the electrode surface (marked by red shadow) in the presence of illumination, and the junction structure shows sp^2 hybridization type before relaxation. **g** sp^3 hybridization after relaxation since the hot electrons can attach to the N atom. **h** The Au-N coordinate covalent bond breaks and sp^2 hybridization occurs when the N atom is stretched out of the distribution of hot electrons. **i** The complete breaking of the molecular junction due to the stretching process under illumination.

Figure 3d and 3e describe the evolution of TPB molecular junction from a connected state to a disconnected state in the absence of illumination, as confirmed by the following calculations. During this stretching process, the anchoring groups triphenylamine remain in the sp^2 hybridization state, because the steric hindrance of the two benzene rings at the end of the molecule blocks the direct coupling between Au and N atoms. As previously reported, the hot electrons can extend further away from the nanoelectrodes than an equilibrium electron distribution[18,46], and subsequently reach the anchoring N atom of the TPB molecule. For a nearby electron acceptor, the hot electrons can efficiently transfer from a plasmonic nanostructure state into the acceptor's electronic states because of their higher energy[42]. Meanwhile, the lone pair of electrons on the N atom forms a coordinate bond with the Au atom *via* the extended hot electrons[47]. Figure 3f-3i present the evolution of the hybridization type of N atom upon illumination during the stretching process. The hot electrons near the surface of the electrodes can attach to the nearby N atom when the gap size is small enough (Fig. 3f), which may result in hybridization switching of the N atom from sp^2 to sp^3 after a

suitable relaxation time (Fig. 3g). During the stretching process, the molecule moves away from the electrodes on the one hand and the local field strength in the nanogap decreases on the other, see supplementary Fig. S5 for more details. On condition that the gap size exceeds the extended proximity range of the hot electrons, the Au-N bond will break and the hybridization state consequently changes back to sp^2 (Fig. 3h). Further stretching will cause the complete breaking of the molecular junction (Fig. 3i). This repeatable process is most likely the reason for the observation of three statistically determined conductance upon illumination, which we will further elaborate in below.

To have an in-depth understanding of our system, we investigated the electron transport through the TPB molecular junctions by means of first-principle calculations. The original structure of the isolated TPB in the absence of electrodes was investigated by optimizing it in Gaussian 09 Package[48]. We found that the N atoms remain in sp^2 hybridization, which means that the gold atoms cannot connect to the N atoms easily due to the steric hindrance of the benzene rings. Therefore, there was only one peak with a low conductance value in the absence of illumination during the stretching processes, and this peak can be attributed to the weak coupling of the benzene rings and electrodes.

Furthermore, quasi-static geometric optimizations with various gap sizes between the electrodes were simulated, which were chosen to describe the dynamic stretching process, so that one can compare geometric structures of different hybridization types. To describe the effect of hot electrons upon light illumination, we set the initial hybridization state of the anchoring structure to sp^3, when the molecules were adsorbed

on the electrode surfaces. In this way, the gold atom on the tip of the electrode can form a coordinate bond with the N atom *via* the lone pair of electrons. The models for the geometric optimization consisted of two-layer Au (100) electrode units and a single TPB molecule bonded to the electrodes on the top sites. The geometric optimizations and electronic structure calculations were performed with the Lanl2DZ basis set in Gaussian 09 package.

By optimizing the structures with various gap sizes, we obtained three types of optimized geometric structures, as presented in Fig. 4. For each gap size in each molecular junction, the dihedral angle (C^1-N-C^2-C^3), *i.e.*, the angle between the plane (C^1-N-C^2) and plane (C^2-N-C^3) as presented in Fig. 3c, varies from 120° to 180°. The trivalent nitrogen atoms could be either sp^2- (N-torsion 180°) or sp^3-hybridized (N-torsion 120°), or could be in an intermediate hybridization state. Our target molecule can connect with the gold electrodes *via* two sp^3-hybridized terminals (dihedral angle is approximately 130°) at both ends as the gap size is 13.08 Å (Fig. 4a and 4d), or *via* an sp^2-hybridized terminal (dihedral angle ~172°) at one end and an sp^3-hybridized terminal (dihedral angle approximately 128°) at the other as the gap size is approximately 13.98 Å (Fig. 4b and 4e), or *via* two sp^2-hybridized terminals (dihedral angle is approximately 169° and 174°) at both ends when the gap size is stretched to 16.58 Å (Fig. 4c and 4f).

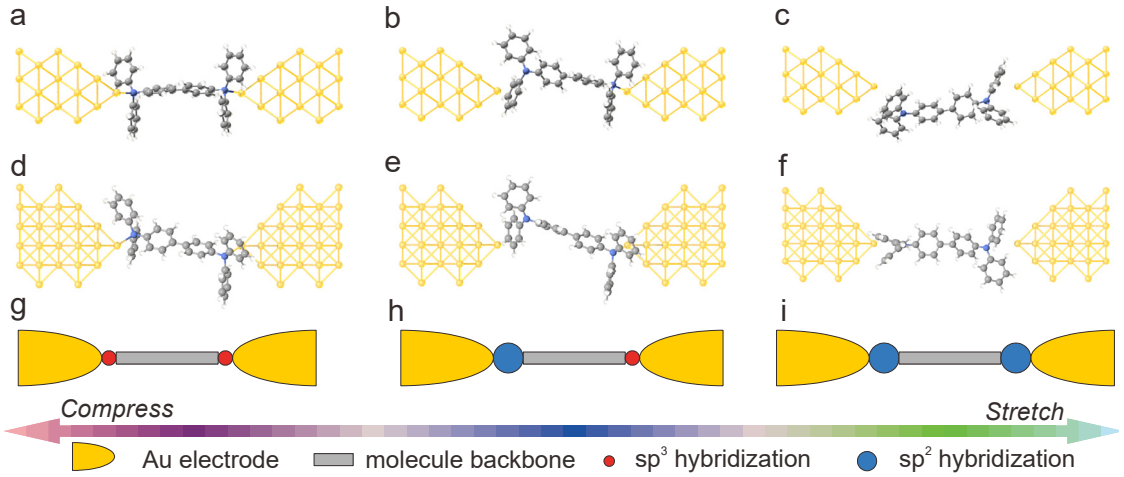

Fig. 4 | Three types of optimized geometric structures with different electrodes gap sizes. (**a-c)** present the front view of the optimized geometric structures with 13.08 Å, 13.98 Å and 16.58 Å gap sizes between electrodes, respectively. The N atoms are marked by blue color. (**d-f)** show the top-front view of the optimized geometric structures with the different gap sizes as presented in (**a-c**). (**g-i)** illustrate the different types of hybridization with different gap sizes, which correspond to the structures presented in (**a-c**).

For convenience, we named these three structures of molecule junction as sp^3-sp^3, sp^3-sp^2 and sp^2-sp^2. Notably, the gold electrode couples with the molecule directly by Au-N bond for the sp^3-hybridized terminals, while the electrode weakly couples with the molecule by π electron *via* the benzene ring for the sp^2-hybridized terminals. When the electrode tip couples with the N atom rather than the benzene ring, the electrons transport across a shorter molecular backbone. The shorter transport path together with a stronger coupling will result in a much larger conductance value, see supplementary Fig. S6.

The transport characteristics of modeled single-molecule junctions were investigated by employing nonequilibrium Green's function (NEGF) method in conjugation with density functional theory (DFT) in TranSIESTA electronic transport package[49,50]. The simulations were performed with the Perdew-Burke-Ernzerhof (PBE) functional in the generalized gradient approximation (PBE-GGA) for exchange-correlation[51]. The current under a finite bias voltage was calculated according to the Landauer-Büttiker formula[52].

$$I = 2e/h \int T(E,V)[f(E-\mu_L) - f(E-\mu_R)]dE \quad (3)$$

where $T(E,V)$ is the transmission coefficient of the electrons at an energy E under a bias voltage V. $f(E-\mu_{L/R})$ is the Fermi-Dirac distribution for electrons at energy E in the left/right electrode with chemical potential $\mu_{L/R}$.

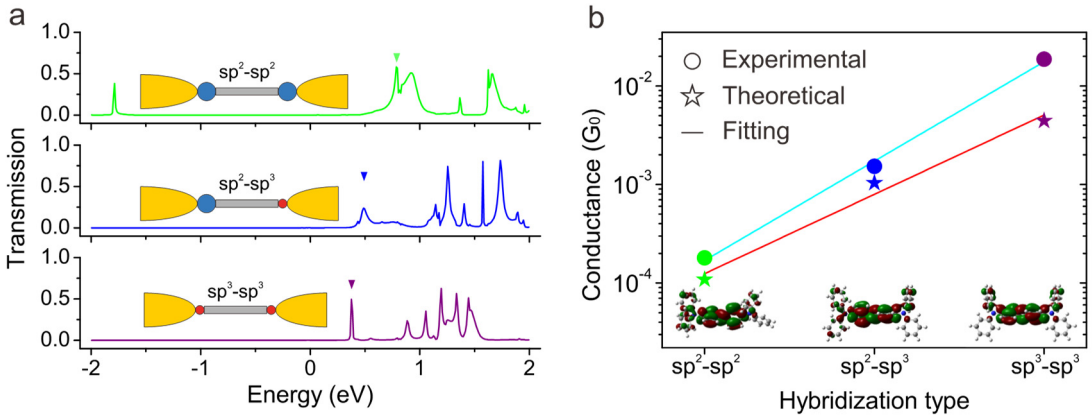

Fig. 5 | Transmission spectra and conductance of TPB molecular junctions. a Transmission spectra of TPB molecular junctions at 0.8 V for sp^2-sp^2 (green), sp^2-sp^3 (blue) and sp^3-sp^3 (purple) structures, respectively. The arrows indicate the shift of the LUMO-dominated transmission peak for different types of junctions. Inset: Schematic of the different types of junctions. **b** Conductance with the logarithm scale as a function

of the hybridization type of molecular junctions. The circles represent experimental data and stars show the data extracted from the theoretical simulations. Inset show the wave function of LUMO with three different type of molecule junctions.

For comparison, we calculated the transmission spectra and the corresponding conductance in the TPB molecular junctions at 0.8 V bias voltage for these three structures. Figure 5a presents the transmission spectra of sp^2-sp^2, sp^2-sp^3 and sp^3-sp^3 structures, respectively. The LUMO-dominated transmission peak of the sp^3-sp^3 structure is the closest to the Fermi level, followed by the transmission peak of the sp^2-sp^3 structure, and finally the transmission peak of the sp^2-sp^2 structure. The conductance of the TPB molecular junctions of sp^2-sp^2, sp^2-sp^3 and sp^3-sp^3 configurations was calculated to be 1.1×10^{-4} G_0, 1.0×10^{-3} G_0, and 4.4×10^{-3} G_0, respectively, as shown in Fig. 5b. The logarithm values of the theoretical conductance exhibit a linear relationship, which means that the calculated molecular conductance values also follow $G_2 \approx \sqrt{G_1 \times G_3}$, in agreement with the experimental results. Notably, the measured conductance data are higher than the theoretically calculated data, and we attribute it to 1) direct transport of plasmon-induced hot carriers through the nanogap or photo-assisted tunneling, which contributes as additional tunneling current[33,36]; 2) as long as stable coordinate bonds between Au and N atoms are established, the hot carriers can extend into the benzene ring and envelop the N atom, thus enhancing the electron transmission[18], which is not taken into consideration in the theoretical calculation. It can also be found that the wave functions for all the three kinds of junction are located on the molecular backbone instead of anchoring groups despite the fact that sp^2

hybridization shows a better conjugated effect, which indicates the anchoring groups contribute a poor conductivity. As mention above, for an sp^3 hybridization anchoring group, the electrode atoms couple with N atom directly, which decreases the length of the scattering region and thus enhances the conductance of the molecule junctions. This observation agree well with the calculated condutance.

Conclusion

In conclusion, a giant photo-induced conductance enhancement is revealed in TPB and TPD molecular junctions by extending our laser-integrated MCBJ setup. Accordingly, a concept that a strong coupling between molecules (with buried anchoring groups) and electrodes may be established *via* plasmon-induced hot electrons is put forward. The large number of hot electrons generated by plasmon excitation broad the spatial distribution of electrons. This effect causes the electrodes to interact with the buried anchoring atoms in the molecules, resulting the changing of the hybridization state. The experimental results agree well with the theoretical predictions calculated by employing density functional theory (DFT) combined with nonequilibrium Green's function (NEGF) method. This work provides a method to modulate molecular conductance by two orders of magnitude *via* light illumination and may promote the development of single molecule-based hybrid optoelectronic devices.

Methods

Chemicals: Poly (pyromellitic dianhydride-co-4,4′-oxydianiline), amic acid solution (PAA) was purchased from Signa-Aldrich, used as a precursor for polyimide coatings. N-methyl-pyrrolidinone (>99% purity) was purchased from Aladdin to dilute PAA for better fluidity. N,N,N′,N′-

tetraphenylbenzidine (98% purity) was purchased from Meryer Technologies and used without further purification. Tetrahydrofuran (99% purity) was purchased from Aladdin.

Acknowledgements

We acknowledge the financial support from the National Natural Science Foundation of China (91950116, 11804170), Natural Science Foundation of Tianjin (19JCZDJC31000, 19JCJQJC60900), National Creative Research Laboratory program (Grant no. 2012026372) through the National Research Foundation of Korea, and the US National Science Foundation (ECCS 2010875).

Author contributions

D. X., T. L. and B. X. initiated the project. Z. Z., T. L. and D. X. designed the experimets. Z. Z. and C. G. perfomed the electrical measument. F. S. and Z. L. executed the optimization simulations and meaured the UV-Vis spectra. Z. Z. and T. N. performed the finite-element simulations for field strengthen in the nanogaps. X. Z. and L. N. helped to prepare the samples for electrical investigations. Q. W. and K. K. contributed to the key comments for upgrading the paper. All authors were involved in the writing of the paper.

Competing interests

The authors declare no competing interests.

Additional information

Supplemantary information is avaliable for this paper at xxxxx

Correspondence and requests for materials should be addressed to D. X. or T. L.

References

1. Aradhya SV, Venkataraman L. Single-molecule junctions beyond electronic transport. *Nat. Nanotechnol.* **8**, 399 (2013).
2. Xiang D, Wang X, Jia C, Lee T, Guo X. Molecular-scale electronics: From concept to function. *Chem. Rev.* **116**, 4318-4440 (2016).
3. Zhang JL*, et al.* Towards single molecule switches. *Chem. Soc. Rev.* **44**, 2998-3022 (2015).
4. Song H, Kim Y, Jang YH, Jeong H, Reed MA, Lee T. Observation of molecular orbital gating. *Nature* **462**, 1039-1043 (2009).
5. Vadai M*, et al.* Plasmon-induced conductance enhancement in single-molecule junctions. *J. Phys. Chem. Lett.* **4**, 2811-2816 (2013).
6. Giguère A, Ernzerhof M, Mayou D. Surface plasmon polariton-controlled molecular switch. *J. Phys. Chem. C* **122**, 20083-20089 (2018).
7. Zhan C, Chen X-J, Yi J, Li J-F, Wu D-Y, Tian Z-Q. From plasmon-enhanced molecular spectroscopy to plasmon-mediated chemical reactions. *Nat. Rev. Chem.* **2**, 216-230 (2018).
8. Barnes WL, Dereux A, Ebbesen TW. Surface plasmon subwavelength optics. *Nature* **424**, 824-830 (2003).
9. Jia C*, et al.* Covalently bonded single-molecule junctions with stable and reversible photoswitched conductivity. *Science* **352**, 1443-1445 (2016).
10. Huang C*, et al.* Single-molecule detection of dihydroazulene photo-thermal reaction using break junction technique. *Nat. Commun.* **8**, 15436 (2017).
11. Tebikachew BE*, et al.* Effect of ring strain on the charge transport of a robust norbornadiene–quadricyclane-based molecular photoswitch. *J. Phys. Chem. C* **121**, 7094-7100 (2017).

12. Darwish N, Aragonès AC, Darwish T, Ciampi S, Díez-Pérez I. Multi-responsive photo- and chemo-electrical single-molecule switches. *Nano Lett.* **14**, 7064-7070 (2014).
13. Dulić D*, et al.* One-way optoelectronic switching of photochromic molecules on gold. *Phys. Rev. Lett.* **91**, 207402 (2003).
14. Kim Y*, et al.* Charge transport characteristics of diarylethene photoswitching single-molecule junctions. *Nano Lett.* **12**, 3736-3742 (2012).
15. Cai S*, et al.* Light-driven reversible intermolecular proton transfer at single-molecule junctions. *Angew. Chem. Int. Ed.* **58**, 3829-3833 (2019).
16. Kohler S, Lehmann J, Hänggi P. Driven quantum transport on the nanoscale. *Phys. Rep.* **406**, 379-443 (2005).
17. Arielly R, Ofarim A, Noy G, Selzer Y. Accurate determination of plasmonic fields in molecular junctions by current rectification at optical frequencies. *Nano Lett.* **11**, 2968-2972 (2011).
18. Fung ED, Adak O, Lovat G, Scarabelli D, Venkataraman L. Too hot for photon-assisted transport: Hot-electrons dominate conductance enhancement in illuminated single-molecule junctions. *Nano Lett.* **17**, 1255-1261 (2017).
19. Galperin M, Nitzan A. Molecular optoelectronics: The interaction of molecular conduction junctions with light. *Phys. Chem. Chem. Phys.* **14**, 9421-9438 (2012).
20. Galperin M, Nitzan A. Optical properties of current carrying molecular wires. *J. Chem. Phys.* **124**, 234709 (2006).
21. Zhou J, Wang K, Xu B, Dubi Y. Photoconductance from exciton binding in molecular junctions. *J. Am. Chem. Soc.* **140**, 70-73 (2018).
22. Mativetsky JM, Pace G, Elbing M, Rampi MA, Mayor M, Samorì P. Azobenzenes as light-controlled

molecular electronic switches in nanoscale metal−molecule−metal junctions. *J. Am. Chem. Soc.* **130**, 9192-9193 (2008).

23. Meng L*, et al.* Side-group chemical gating via reversible optical and electric control in a single molecule transistor. *Nat. Commun.* **10**, 1450 (2019).
24. Tam ES*, et al.* Single-molecule conductance of pyridine-terminated dithienylethene switch molecules. *ACS Nano* **5**, 5115-5123 (2011).
25. Bei Z, Huang Y, Chen Y, Cao Y, Li J. Photo-induced carbocation-enhanced charge transport in single-molecule junctions. *Chem. Sci.* **11**, 6026-6030 (2020).
26. Guhr DC, Rettinger D, Boneberg J, Erbe A, Leiderer P, Scheer E. Influence of laser light on electronic transport through atomic-size contacts. *Phys. Rev. Lett.* **99**, 086801 (2007).
27. Ittah N, Selzer Y. Electrical detection of surface plasmon polaritons by 1g0 gold quantum point contacts. *Nano Lett.* **11**, 529-534 (2011).
28. Chen L*, et al.* Towards single-molecule optoelectronic devices. *Sci. China Chem.* **61**, 1368-1384 (2018).
29. Zayats AV, Smolyaninov II, Maradudin AA. Nano-optics of surface plasmon polaritons. *Phys. Rep.* **408**, 131-314 (2005).
30. Han Z, Bozhevolnyi SI. Radiation guiding with surface plasmon polaritons. *Reports on Progress in Physics* **76**, 016402 (2012).
31. Savage KJ, Hawkeye MM, Esteban R, Borisov AG, Aizpurua J, Baumberg JJ. Revealing the quantum regime in tunnelling plasmonics. *Nature* **491**, 574-577 (2012).
32. Zhang W*, et al.* Atomic switches of metallic point contacts by plasmonic heating. *Light Sci. Appl.* **8**, (2019).

33. Vadai M, Selzer Y. Plasmon-induced hot carriers transport in metallic ballistic junctions. *J. Phys. Chem. C* **120**, 21063-21068 (2016).
34. Venkataraman L, Klare JE, Nuckolls C, Hybertsen MS, Steigerwald ML. Dependence of single-molecule junction conductance on molecular conformation. *Nature* **442**, 904-907 (2006).
35. Wu J-T, Hsiang T-L, Liou G-S. Synthesis and optical properties of redox-active triphenylamine-based derivatives with methoxy protecting groups. *J. Mater. Chem. C* **6**, 13345-13351 (2018).
36. Selzer Y, Cabassi MA, Mayer TS, Allara DL. Thermally activated conduction in molecular junctions. *J. Am. Chem. Soc.* **126**, 4052-4053 (2004).
37. Lin L*, et al.* Electron transport across plasmonic molecular nanogaps interrogated with surface-enhanced raman scattering. *ACS Nano* **12**, 6492-6503 (2018).
38. Breit G, Wigner E. Capture of slow neutrons. *Phys. Rev.* **49**, 519-531 (1936).
39. Lambert CJ. Basic concepts of quantum interference and electron transport in single-molecule electronics. *Chem. Soc. Rev.* **44**, 875-888 (2015).
40. Furube A, Hashimoto S. Insight into plasmonic hot-electron transfer and plasmon molecular drive: New dimensions in energy conversion and nanofabrication. *NPG Asia Mater.* **9**, e454-e454 (2017).
41. Natelson D, Evans C, Zolotavin P. Photovoltages and hot electrons in plasmonic nanogaps. In: *Quantum Sensing and Nano Electronics and Photonics XV* eds Razeghi M, Brown GJ, Lewis JS, Leo G. (2018).
42. Mukherjee S*, et al.* Hot electrons do the impossible: Plasmon-induced dissociation of h2 on au. *Nano Lett.* **13**, 240-247 (2013).
43. Kazuma E, Jung J, Ueba H, Trenary M, Kim Y. Real-space and real-time observation of a plasmon-induced chemical reaction of a single molecule. *Science* **360**, 521-526 (2018).

44. Tame MS, McEnery KR, Özdemir ŞK, Lee J, Maier SA, Kim MS. Quantum plasmonics. *Nat. Phys.* **9**, 329-340 (2013).
45. Zuloaga J, Prodan E, Nordlander P. Quantum description of the plasmon resonances of a nanoparticle dimer. *Nano Lett.* **9**, 887-891 (2009).
46. Weng Q*, et al.* Imaging of nonlocal hot-electron energy dissipation via shot noise. *Science* **360**, 775-778 (2018).
47. Sugita Y, Taninaka A, Yoshida S, Takeuchi O, Shigekawa H. The effect of nitrogen lone-pair interaction on the conduction in a single-molecule junction with amine-au bonding. *Sci. Rep.* **8**, 5222 (2018).
48. Frisch MJ*, et al. Gaussian 09 rev. D.01* (2009).
49. Soler JM*, et al.* The siesta method forab initioorder-nmaterials simulation. *J. Phys.: Condens. Matter* **14**, 2745-2779 (2002).
50. Stokbro K, Taylor J, Brandbyge M, OrdejÓN P. Transiesta: A spice for molecular electronics. *Ann. N. Y. Acad. Sci.* **1006**, 212-226 (2003).
51. Perdew JP, Burke K, Ernzerhof M. Generalized gradient approximation made simple. *Phys. Rev. Lett.* **77**, 3865-3868 (1996).
52. Datta S, Ahmad H, Pepper M. *Electronic transport in mesoscopic systems*. Cambridge University Press (1997).

Table of Contents:

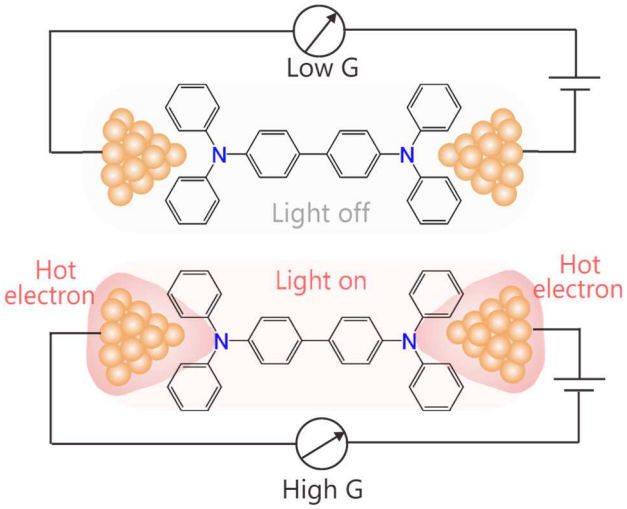

A giant conductance enhancement: the conductance of nonphotoresponsive molecules can be enhanced by two orders of magnitudes *via* light illumination, which results from the coupling of plasmon-excited hot electrons and the buried anchoring group.

Figures

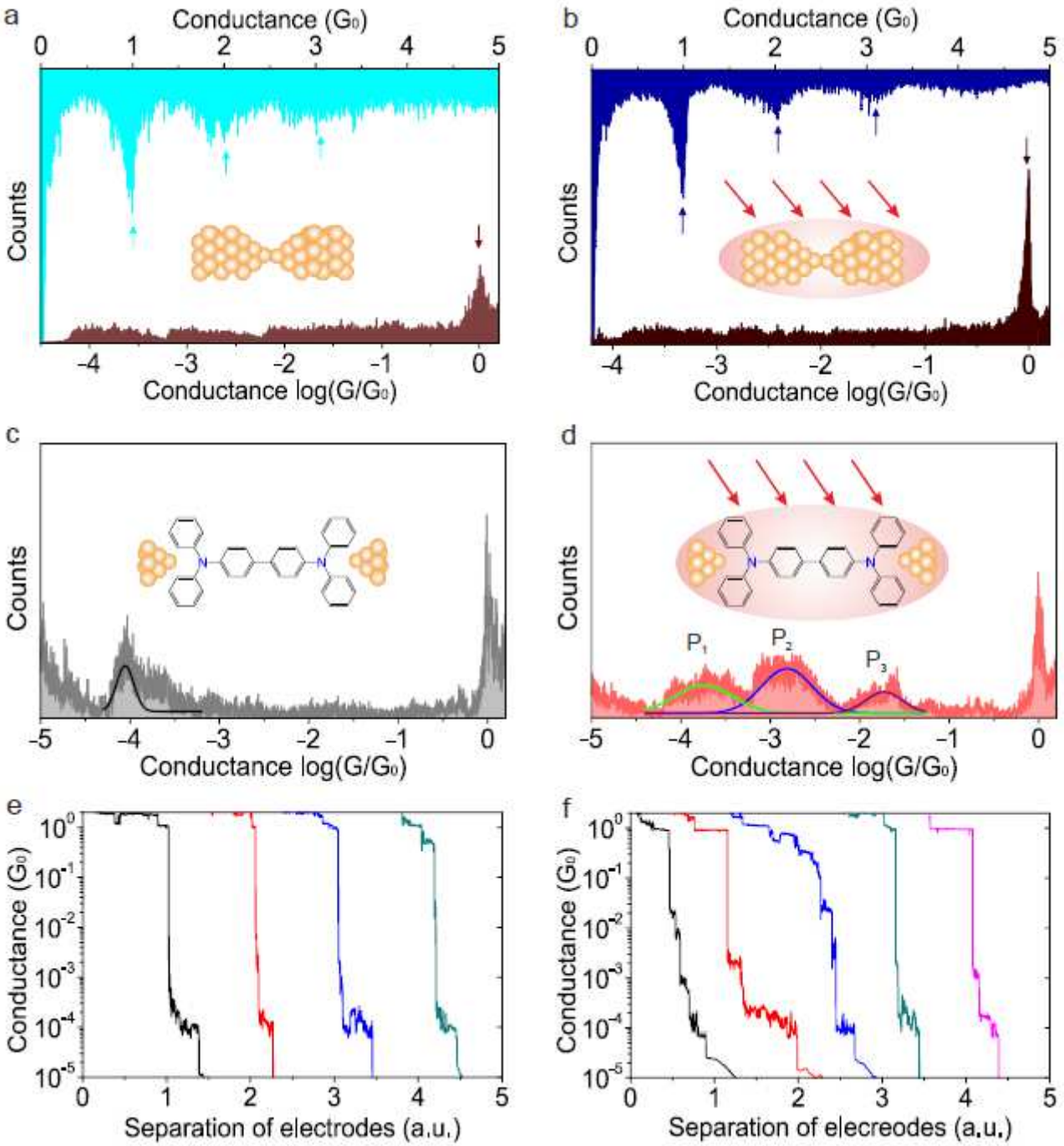

Figure 1

Conductance traces and histograms of the junctions with and without light illumination. (a-b) Linear and logarithm conductance histograms of bare gold wire (a) in dark and (b) upon illumination. c Conductance histogram of TPB molecules sandwiched between two electrodes in the absence of illumination with a Gaussian fitted peak at approximately 8.8×10-5 G0. Inset: Schematic of the molecular structure sandwiched between two separated electrodes. d Conductance histogram of TPB molecules in the

presence of illumination, with three Gaussian-fitted peaks (P1, P2, and P3) at approximately 1.8×10-4 1 G0, 1.5×10-3 G0, and 1.9×10-2 G0, respectively. (e-f) Logarithm conductance traces during the separation of the electrodes (e) without laser illumination and (f) in the presence of illumination.

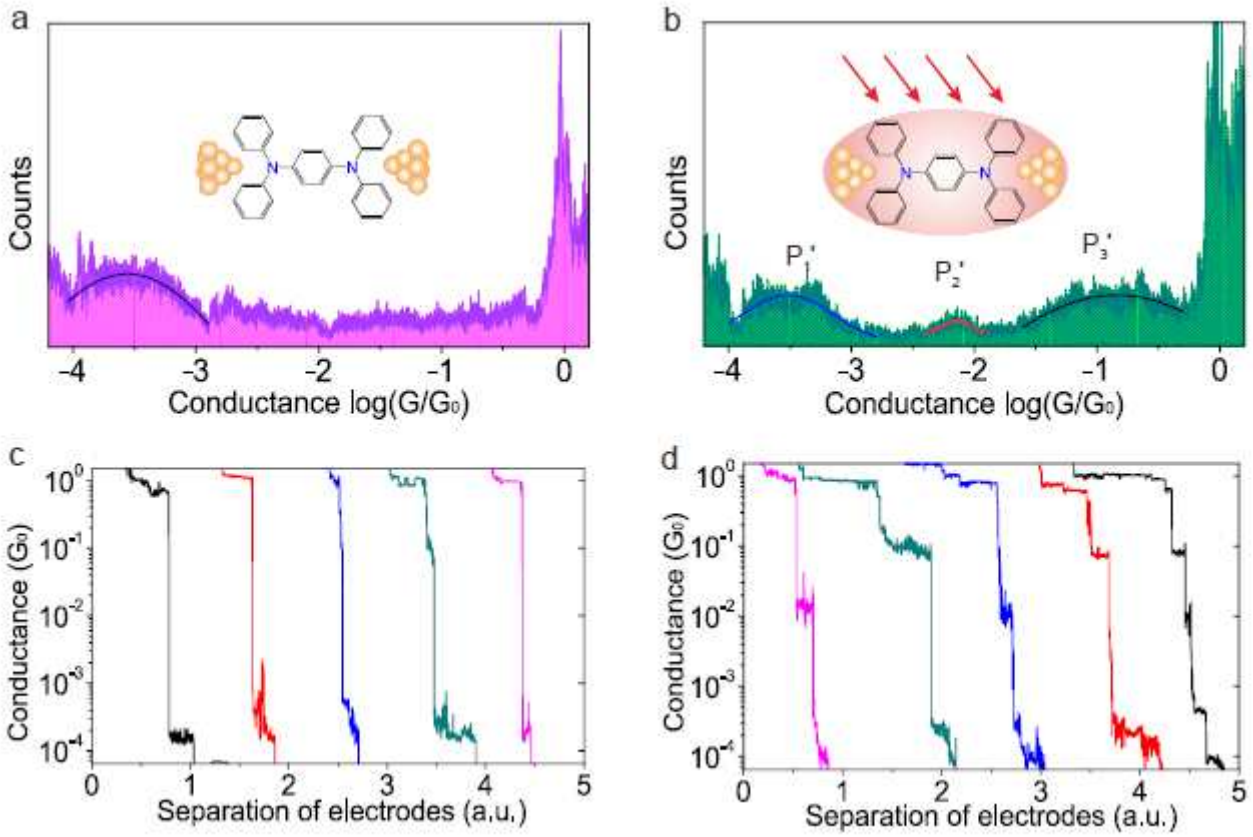

Figure 2

Conductance traces and histograms of the TPD junctions with and without light illumination. a Conductance histogram of TPD molecules in dark condition, with a Gaussian-fitted peak at approximately 2.8×10-4 G0. The inset illuminates the molecular structure sandwiched between two separated electrodes. b Conductance histogram of TPD molecules upon illumination with three Gaussian-fitted peaks (P1', P2', and P3') at approximately 3.0×10-4 G0, 7.2×10-3 G0, and 9.8×10-2 G0, respectively. (c-d) Logarithm conductance traces during the separation of electrodes (c) without light illumination and (d) upon illumination.

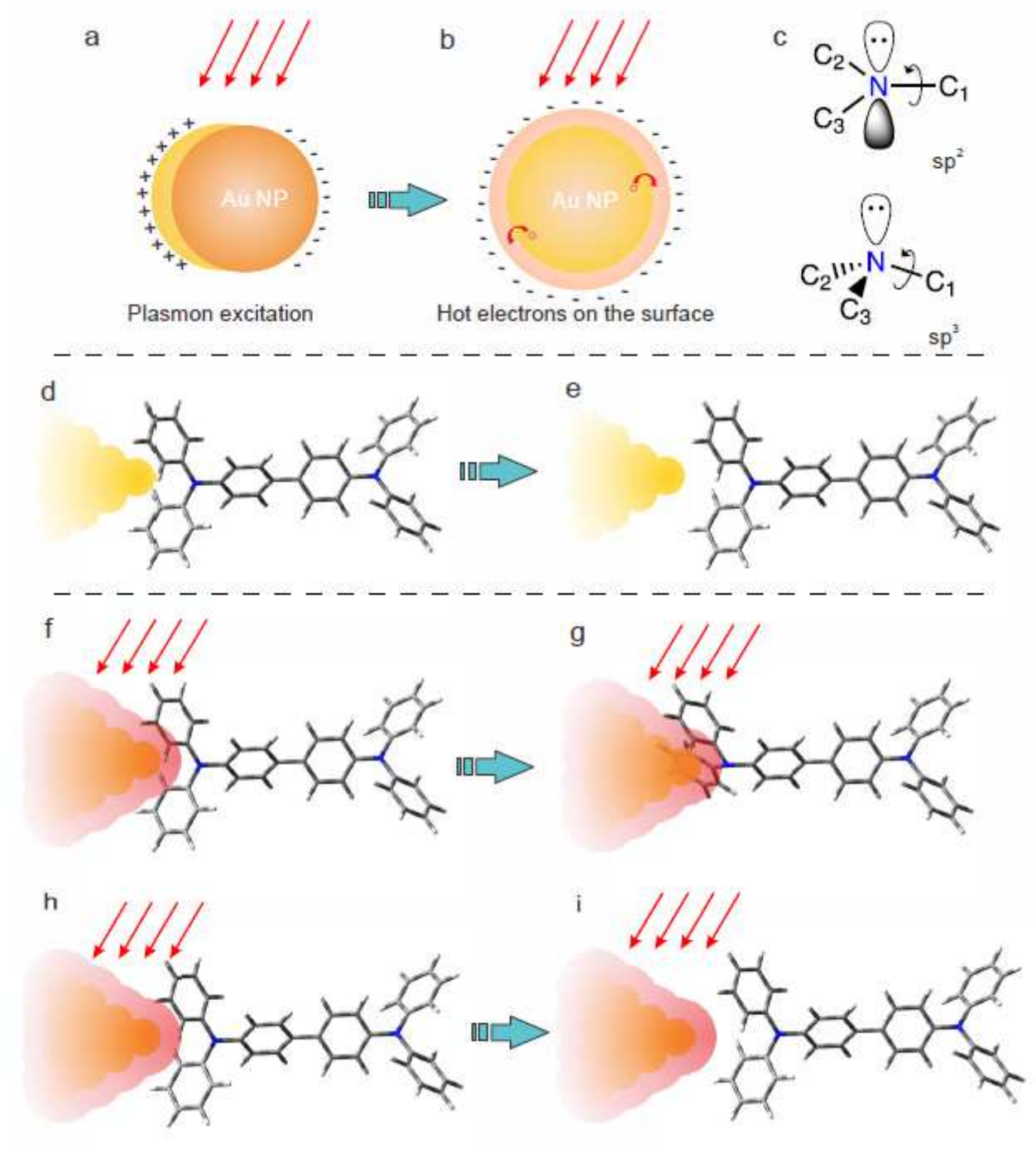

Figure 3

Schematics of the generation of hot electrons on gold nanoparticle surface and the change of orbital hybridization of N atom upon illumination. a Plasmon excited gold nanoparticles as an efficient source of hot electrons. b The expanded distribution of hot electrons on the surface of the nanoparticles. c The dihedral angle of N atom in sp2(180°) and sp3(120°) hybridization state. d The initial junction structure without laser illumination. Only one electrode is shown in the molecule junction. e The breaking of the molecular junction during the stretching process in the dark. f The distribution 1 of hot electrons expanded beyond the electrode surface (marked by red shadow) in the presence of illumination, and the junction structure shows sp2 hybridization type before relaxation. g sp3 hybridization after relaxation

since the hot electrons can attach to the N atom. h The Au-N coordinate covalent bond breaks and sp2 hybridization occurs when the N atom is stretched out of the distribution of hot electrons. i The complete breaking of the molecular junction due to the stretching process under illumination.

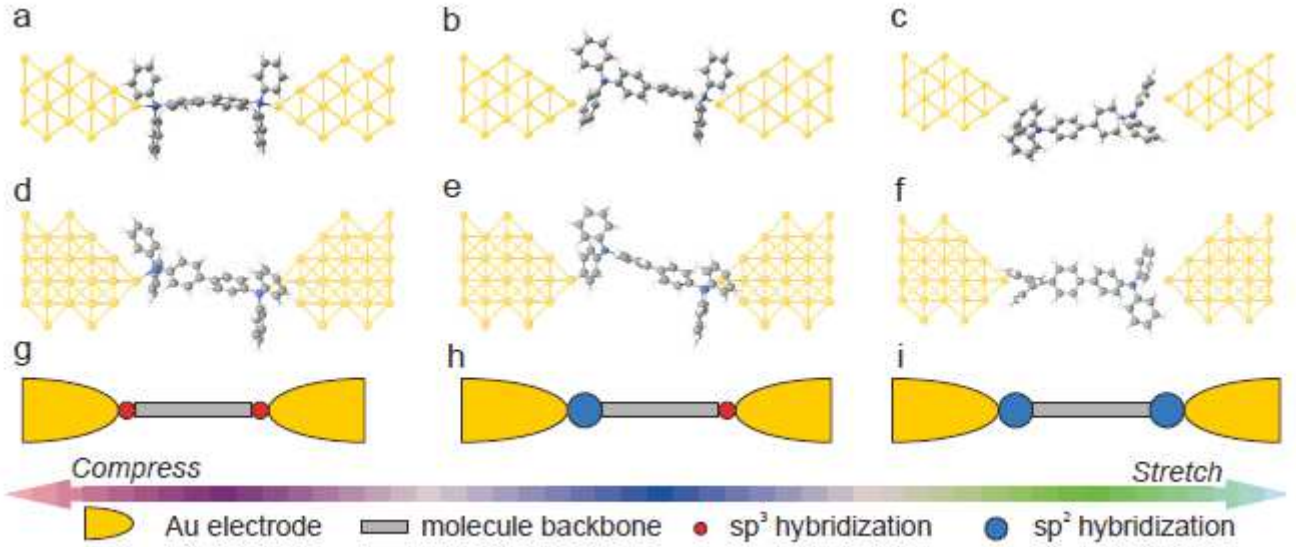

Figure 4

Three types of optimized geometric structures with different electrodes gap sizes. (a-c) present the front view of the optimized geometric structures with 13.08 Å, 13.98 Å and 16.58 Å gap sizes between electrodes, respectively. The N atoms are marked by blue color. (d-f) show the top-front view of the optimized geometric structures with the different gap sizes as presented in (a-c). (g-i) illustrate the different types of hybridization with different gap sizes, which correspond to the structures presented in (a-c).

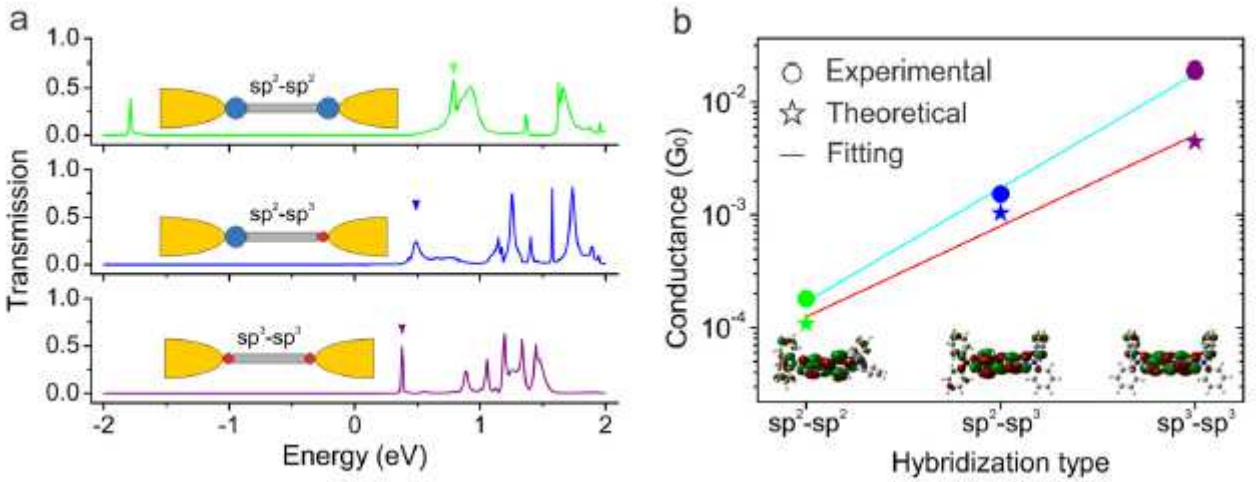

Figure 5

Transmission spectra and conductance of TPB molecular junctions. a Transmission spectra of TPB molecular junctions at 0.8 V for sp2-sp2 (green), sp2-sp3 (blue) and sp3-sp3 (purple) structures,

respectively. The arrows indicate the shift of the LUMO-dominated transmission peak for different types of junctions. Inset: Schematic of the different types of junctions. b Conductance with the logarithm scale as a function of the hybridization type of molecular junctions. The circles represent experimental data and stars show the data extracted from the theoretical simulations. Inset show the wave function of LUMO with three different type of molecule junctions.

Supplementary Files

This is a list of supplementary files associated with this preprint. Click to download.

- SupplementaryinfromationZhao.pdf